

InSAR-based assessment of land subsidence and its relationship with groundwater extraction

Swati Mishra*
Research Scholar, Department of Agriculture, International Institute of Information Technology Hyderabad, Hyderabad, Telangana, India

Corresponding Author: Swati Mishra

Volume: 1, Issues: 1, Year: 2026, Page No.: 1-8

Receive Date: 21-08-2026**; Accept Date:** 05-10-2026**; Published Date:** 20-10-2026

Abstract
Land subsidence caused by groundwater withdrawal is a slow, spatially extensive hazard that damages buildings, pipelines, transport corridors, and flood defenses, and it permanently reduces aquifer storage. Satellite interferometric synthetic aperture radar (InSAR) now measures this deformation at millimeter precision, over thousands of square kilometers, and at repeat intervals of days to weeks. This paper presents a structured framework for turning InSAR deformation records into a quantitative assessment of how groundwater extraction drives subsidence. The framework has four stages: acquisition and time-series processing, error control, hydrogeological interpretation, and risk classification. The text synthesizes published findings from Las Vegas, Mexico City, Jakarta, Mashhad, Beijing, and northern India to show what InSAR reveals about the aquifer-system response. It also identifies the main sources of uncertainty. The paper does not report newly processed satellite data. The worked example in Section 6 is a labeled, illustrative calculation, not a measured result. The central argument is that InSAR yields its strongest hydrogeological information when displacement is treated as a physical response variable, interpreted jointly with groundwater head, lithology, and pumping history, rather than as a standalone map.

Keywords: InSAR, land subsidence, groundwater extraction, aquifer compaction, Sentinel-1, time-series analysis, skeletal storage

Introduction

When water is removed from a confined or semi-confined aquifer system faster than it is replenished, pore-fluid pressure falls. The weight of the overlying sediments, formerly shared between the pore water and the grain skeleton, shifts onto the skeleton, and the sediments compact. Fine-grained layers such as clays and silts compact the most and release their water slowly. A large portion of this compaction is inelastic, meaning it does not reverse when water levels recover. The surface above the aquifer therefore sinks, and the lost pore space cannot be restored (Poland, 1984; Galloway *et al.*, 1999) [1, 2].

The problem is global and growing. A worldwide susceptibility analysis concluded that subsidence-prone ground overlaps with a large and increasing share of the human population, with groundwater depletion in irrigated plains and expanding cities as the leading driver (Herrera-García *et al.*, 2021) [3]. Satellite gravimetry has documented severe depletion in northern India (Rodell *et al.*, 2009) [4], and global hydrological modeling shows that groundwater abstraction has outpaced recharge in many large aquifer systems (Wada *et al.*, 2010) [5]. Coastal cities face an additional threat, because subsidence adds directly to sea-level rise as a cause of relative flooding hazard (Shirzaei *et al.*, 2021) [6].

Traditional monitoring relies on leveling surveys, extensometers, and continuous GNSS stations. These instruments are accurate but sparse, expensive, and labor-intensive, so they often miss the spatial structure of the deformation field. InSAR fills this gap. Since early demonstrations in hydrogeology (Galloway & Hoffmann, 2007) [7], it has become the primary tool for mapping subsidence at regional scale.

1. How reliably can modern InSAR time-series methods resolve groundwater-related deformation?
2. What does the relationship between displacement and hydraulic head reveal about aquifer properties?
3. How can the results be organized into a defensible assessment of hazard and groundwater sustainability?

Physical Basis

1. Effective stress and aquifer compaction

The governing principle is Terzaghi's effective stress concept (Terzaghi, 1925) [8]. The total stress σ at a given depth is carried partly by pore-water pressure p and partly by the grain skeleton:

$$\sigma' = \sigma - p$$

When pumping lowers p, σ′ increases by the same amount, because σ is essentially unchanged. The resulting vertical compaction of a layer of thickness b_o can be written as

$$\Delta b = S_{ske} \times b_o \times \Delta h$$

Where S_{ske} is the skeletal specific storage (units of inverse length) and Δh is the decline in hydraulic head. Two regimes matter. Below the previous minimum head (the preconsolidation head), the skeleton behaves elastically and S_{ske} is small, so deformation is largely recoverable. Once heads fall beneath the preconsolidation threshold, the skeleton enters the inelastic regime, where S_{ske} can be one to two orders of magnitude larger and compaction is permanent.

2. Delayed drainage

Thick aquitards equilibrate slowly. The characteristic time for a clay layer to adjust to a head change scales with the square of its drainage path length divided by its hydraulic diffusivity. As a result, compaction can continue for years after pumping slows, and surface deformation may lag behind head changes. This lag is a hydrogeological signature that InSAR time series can help reveal, particularly when compared with well hydrographs.

3. Seasonal elastic cycles

In many aquifer systems the head falls during the pumping season and recovers during the off-season. The surface subsides and rebounds in step with this cycle. Studies in the Las Vegas Valley showed that this elastic seasonal signal, superimposed on the long-term inelastic trend, can be separated by InSAR time series (Hoffmann *et al.*, 2001; Bell *et al.*, 2008) [9, 10].

InSAR Measurement Principles

1. From phase to displacement

A SAR satellite transmits a microwave pulse and records the amplitude and phase of the backscattered signal. When two acquisitions of the same area are combined, the phase difference of each pixel encodes the change in slant-range distance between satellite and ground, plus several unwanted terms (Massonnet & Feigl, 1998; Bürgmann *et al.*, 2000) [11, 12]. The deformation component of the phase is related to line-of-sight (LOS) displacement by

$$d_{LOS} = \frac{\lambda}{4\pi} \times \Delta\varphi_{def}$$

Where λ is the radar wavelength. For C-band sensors such as Sentinel-1, λ is about 5.6 cm, so a full 2π phase cycle corresponds to roughly 2.8 cm of LOS motion. Because land subsidence is predominantly vertical, the LOS value is commonly projected to vertical using the local incidence angle θ:

$$d_{vertical} \approx \frac{d_{LOS}}{\cos\theta}$$

This projection assumes negligible horizontal motion, which is generally acceptable for pumping-induced subsidence away from the margins of the subsiding bowl.

2. Decorrelation and its consequences

Interferometric phase is usable only when the scattering properties of a pixel remain stable between acquisitions. Temporal decorrelation, from vegetation growth, plowing, and surface moisture change, and geometric decorrelation, from large perpendicular baselines, reduce coherence (Zebker & Villasenor, 1992) [13]. This is the main reason agricultural basins, where much groundwater is extracted, are harder to monitor than cities, and why C-band results over cropland often need careful pixel selection or longer-wavelength (L-band) data.

3. Time-series algorithms

Two major families dominate:

- **Persistent scatterer (PS):** Methods identify individual pixels dominated by a single stable scatterer, such as buildings, bridges, and rock outcrops, and estimate displacement at those points with high precision (Ferretti *et al.*, 2001; Hooper *et al.*, 2004) [14, 15].
- **Small baseline (SBAS):** Methods form many interferograms with short temporal and spatial baselines and invert them into a displacement time series, preserving more distributed targets (Berardino *et al.*, 2002) [16].

Combined strategies exploit both kinds of targets (Hooper, 2008) [17]. Phase unwrapping, which restores integer cycle ambiguities, is a further critical step; errors there can introduce artificial offsets that look like deformation (Chen & Zebker, 2001) [18]. Careful filtering of the interferometric phase also improves unwrapping reliability (Goldstein & Werner, 1998) [19].

4. Sensors and data availability

Table 1: Radar sensors commonly used for subsidence studies

Sensor / Mission	Band	Approx. wavelength	Typical repeat cycle	Notes for groundwater studies
ERS-1/2, Envisat	C	5.6 cm	35 days	Historical archive from the 1990s; useful for long baselines
ALOS-1 PALSAR	L	23.6 cm	46 days	Better coherence over vegetated farmland
Sentinel-1	C	5.6 cm	6 to 12 days	Free, open, systematic global coverage (Torres *et al*., 2012) [20]
TerraSAR-X / COSMO-SkyMed	X	3.1 cm	4 to 11 days	High resolution; strong in urban areas, weaker in vegetation

Note: Repeat cycles vary with satellite constellation status and acquisition plans.

The free, systematic coverage of Sentinel-1 has been transformative. A decade of consistent acquisitions now allows basin-wide time series at 12-day or shorter intervals, which is fine enough to resolve seasonal pumping cycles.

Methodological Framework

The proposed workflow has four stages, summarized schematically in Figure 1 (see Section 9 for figure descriptions).

Stage 1: Data selection and processing

Select an acquisition stack of at least 30 to 50 scenes from a single track to support robust statistics, and use a consistent geometry (ascending or descending). Form interferograms, correct for topography with a digital elevation model, and apply orbital refinement. Estimate the deformation time series with PS, SBAS, or a combined approach.

Stage 2: Error budgeting

Each InSAR time series contains the signal plus several error terms:

- Atmospheric delay, which has a turbulent component and a topography-correlated stratified component. These can be mitigated by spatiotemporal filtering and, where available, weather-model corrections.
- Orbital and reference errors, usually treated by estimating and removing a long-wavelength ramp and choosing a stable reference region.
- Unwrapping errors, checked through closure-loop analysis.
- DEM error, which scales with the perpendicular baseline.

Residual uncertainty should be reported as a value, ideally by comparing InSAR rates against independent GNSS or leveling benchmarks. Without such validation, a subsidence map is a qualitative product rather than a measurement.

Stage 3: Hydrogeological interpretation

This is the stage in which the assessment becomes more than deformation mapping. Three analyses are central:

- **Spatial correlation:** Overlay deformation rates with pumping-well density, well-field locations, aquifer thickness, and clay fraction.
- **Temporal correlation:** Compare InSAR time series with hydrographs at nearby wells, looking for lag, seasonal amplitude, and hysteresis.
- **Parameter estimation:** Regress compaction against head change to estimate an effective storage coefficient (Section 5).

Stage 4: Risk classification

Combine the deformation rate, cumulative displacement, differential subsidence (which controls structural damage), and exposure of infrastructure into a classified hazard map. A practical set of classes is given in Table 2.

Table 2: Illustrative subsidence hazard classes (screening thresholds)

Class	Vertical rate (mm/yr)	Typical management response
Negligible	< 5	Routine monitoring
Low	5 to 15	Add wells to the monitoring network; review abstraction permits
Moderate	15 to 50	Restrict new abstraction; inspect critical structures
High	50 to 150	Active demand management; managed recharge; infrastructure retrofit
Severe	> 150	Emergency measures and phased pumping reduction

Note: Thresholds are screening values for illustration. Local engineering tolerances and differential-settlement criteria should replace them in any formal assessment.

Linking Displacement to Groundwater Extraction

1. Stress-strain relationships

A powerful diagnostic is the cross-plot of cumulative displacement against head change. In an elastic regime, the relationship is approximately linear and reversible, and the slope gives an elastic skeletal storage estimate. In an inelastic regime the slope steepens and hysteresis appears: displacement does not return along the same path when head recovers. This approach has been used to separate recoverable and permanent components of aquifer-system deformation (Hoffmann *et al.*, 2001; Bell *et al.*, 2008) [9, 10]. Figure 2 illustrates the concept.

2. Structural control

Subsidence rarely follows a simple bowl shape. Faults, buried bedrock highs, and facies changes can act as hydraulic barriers or mechanical hinges. InSAR in the Las Vegas Valley revealed that faults partition the subsidence field and produce sharp displacement gradients that coincide with known fault traces (Amelung *et al.*, 1999) [21]. Such differential motion is an important hazard, because tilting and cracking damage structures far more than uniform settling does.

3. Comparative evidence

Published studies from different hydrogeological settings show a consistent pattern: where groundwater extraction is intense and compressible sediments are thick, InSAR detects subsidence that matches the spatial footprint of the well fields. Table 3 compares selected cases.

Table 3: Selected InSAR studies of groundwater-related subsidence

Region	Setting	Principal finding	Source
Las Vegas Valley, USA	Basin-fill aquifer, managed recharge	Seasonal elastic cycle superimposed on long-term trend; fault-bounded deformation	Amelung *et al*., 1999; Hoffmann *et al*., 2001; Bell *et al*., 2008
Mexico City, Mexico	Lacustrine clay aquitard, heavy pumping	Very high localized rates, with subsidence reaching tens of centimeters per year	Chaussard *et al*., 2014
Jakarta and Semarang, Indonesia	Coastal alluvium, groundwater and gas extraction	Rapid urban subsidence, in places greater than 20 cm/yr	Chaussard *et al*., 2013
Mashhad, Iran	Intermountain valley, agricultural abstraction	Large subsiding area confirmed with leveling and GPS	Motagh *et al*., 2007
Northern Beijing Plain, China	Alluvial plain, deep aquifers	Subsidence tied to groundwater drawdown and lithology	Zhu *et al*., 2015
Bangkok, Thailand	Coastal clay sequence	Historic deep-well pumping caused extensive subsidence, later moderated by regulation	Phien-wej *et al*., 2006

Two lessons stand out. First, policy matters. Where abstraction has been regulated, as in Bangkok, deformation rates have slowed, although the inelastic loss in storage is not recovered. Second, the same InSAR product can serve engineering, hydrogeological, and regulatory audiences, but only if uncertainty and lithological context are reported.

4. Regional context for India

Satellite gravimetry indicated severe depletion in northern India during 2002 to 2008, with the loss attributed mostly to irrigation pumping (Rodell *et al.*, 2009) [4]. Because many Indo-Gangetic aquifers contain interbedded clays, the conditions for compaction exist wherever water levels fall steeply. Systematic InSAR monitoring of such regions would complement well-level observations that are currently sparse relative to the number of abstraction points. Any such program should use L-band data or careful PS selection where cropland dominates, as noted in Section 3.2.

Illustrative Worked Example

The numbers below are hypothetical, chosen to demonstrate the calculation. They are not measurements from any real site.

Suppose a confined aquifer system contains a compressible clay-rich interval with total thickness b_0 = 80 m. Over a five-year period, monitoring wells show an average head decline of 12 m, and InSAR-derived vertical subsidence at the corresponding location totals 0.24 m.

Rearranging the compaction equation gives an effective skeletal specific storage:

$$S_{ske} = \frac{\Delta b}{b_0 \times \Delta h} = \frac{0.24}{80 \times 12} = 2.5 \times 10^{-4}\ m^{-1}$$

An effective S_{ske} of this magnitude is consistent with a system that has entered, or is approaching, a partly inelastic regime. If a later year shows head recovery of 3 m accompanied by only 0.01 m of rebound, the ratio of recovered to total deformation is small, and the compaction should be classified as predominantly permanent. The practical conclusion is that further drawdown below the current minimum head would produce irreversible storage loss, so pumping limits tied to a threshold head would be justified.

This example also shows why independent head data are indispensable. InSAR alone provides Δb, but not Δh, so the physical interpretation depends on wells.

Uncertainty and Limitations

- **Single-geometry bias:** One look direction measures only one projection of the 3-D motion. Combining ascending and descending tracks allows vertical and east-west components to be separated.
- **Incomplete spatial coverage:** PS methods may return few points over farmland or forest, which can leave the most heavily pumped areas unmeasured.
- **Deformation not caused by pumping:** Natural sediment compaction, tectonic motion, mining, oil and gas extraction, and loading by new construction all produce surface motion. Attribution to groundwater requires temporal and spatial evidence, not just co-location. In Jakarta, for example, gas extraction complicates interpretation (Chaussard *et al.*, 2013) [22].
- **Gradient limits:** Very rapid deformation can exceed the maximum phase gradient that C-band sensors can unwrap, so extreme subsidence zones may be underestimated.
- **Short records:** A few years of data may capture seasonal behavior but not the long-term inelastic trend. Merging archival sensors with Sentinel-1 data extends the record, but requires careful reference-frame consistency.
- **Parameter non-uniqueness:** Different combinations of aquitard thickness and compressibility can produce similar displacement curves, so independent geological information should constrain any inversion.

Discussion and Recommendations

Several practical recommendations follow from the evidence synthesized here.

Treat InSAR as one component of a monitoring network: The most defensible assessments pair satellite deformation with well hydrographs, a small number of GNSS or extensometer stations for validation, and lithological logs. This combination converts a deformation map into a calibrated hydromechanical model.

Report uncertainty explicitly: Every rate should carry an error estimate and a statement of the reference point and validation data. This transparency is what allows regulators and engineers to rely on the product.

Use thresholds in head, not only in rate: Because inelastic compaction begins when head drops below its historic minimum, the most useful regulatory variable is often a minimum allowable head at index wells. InSAR then serves to verify that the threshold is protecting the aquifer system.

Prioritize differential subsidence for infrastructure: Differential settlement across faults or facies boundaries, rather than total subsidence, determines structural damage, so gradient maps should accompany rate maps.

Plan for permanence: Managed aquifer recharge can slow or halt compaction, but cannot restore storage lost through inelastic deformation. Management should therefore aim to prevent further drawdown past critical heads, not to depend on later recovery.

Exploit open data: Because Sentinel-1 coverage is free and systematic, even data-poor regions can build baseline subsidence inventories. This is especially relevant for rapidly growing cities in South and Southeast Asia, where pumping is intense and monitoring networks are limited.

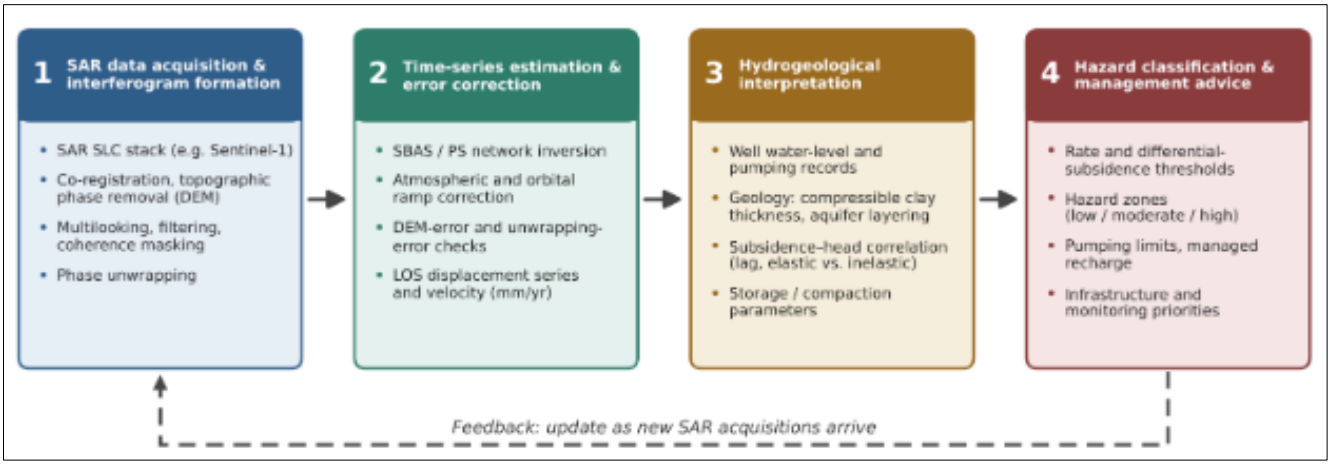

Fig 1: Workflow for InSAR-based assessment of groundwater-related subsidence. A flowchart with four horizontal blocks connected by arrows: (1) SAR data acquisition and interferogram formation; (2) time-series estimation and error correction; (3) hydrogeological interpretation with well data and geology; (4) hazard classification and management advice. A feedback arrow from block 4 to block 1 indicates updating as new acquisitions arrive.

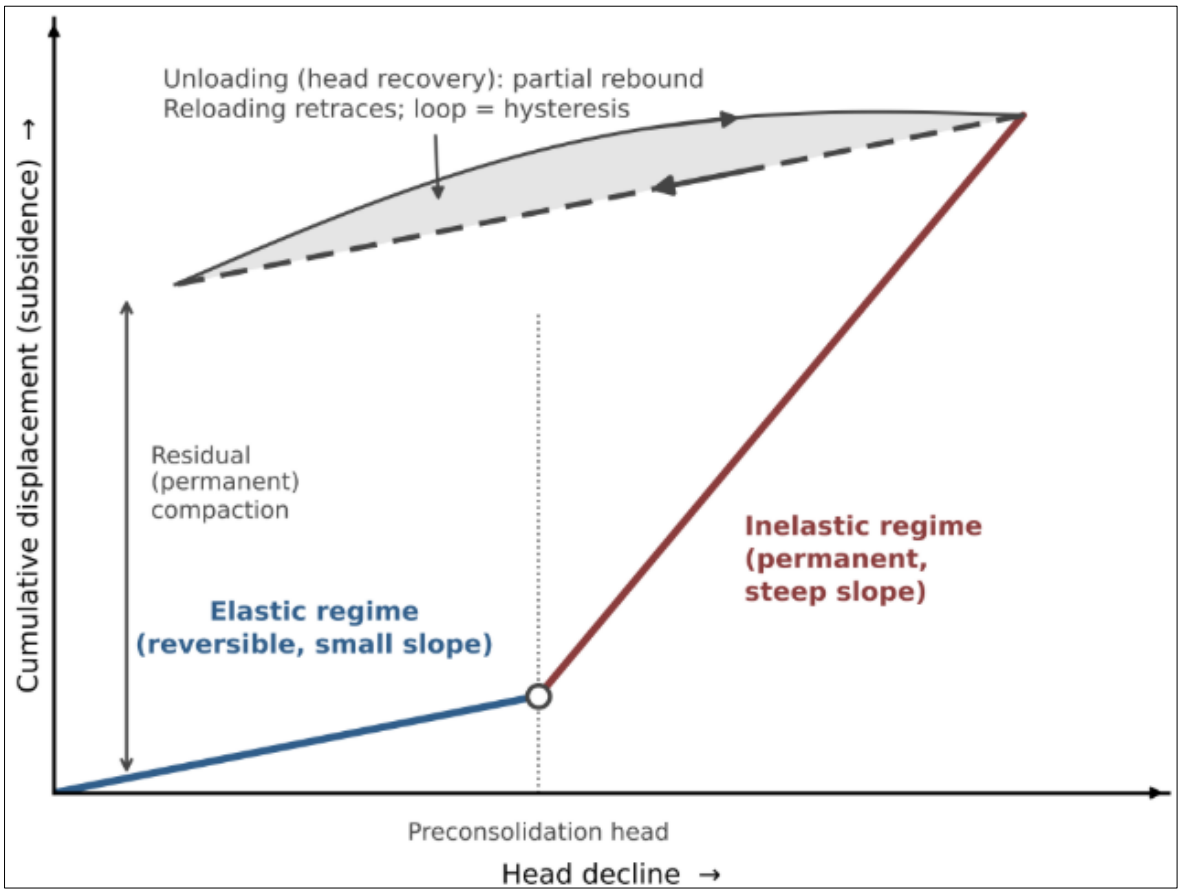

Fig 2: Conceptual stress-strain relationship between head decline and compaction. A plot with head decline on the horizontal axis and cumulative displacement on the vertical axis. A shallow, reversible line labeled "elastic regime" bends at the preconsolidation head into a steeper line labeled "inelastic regime." A return path on recovery shows only partial rebound, forming a hysteresis loop.

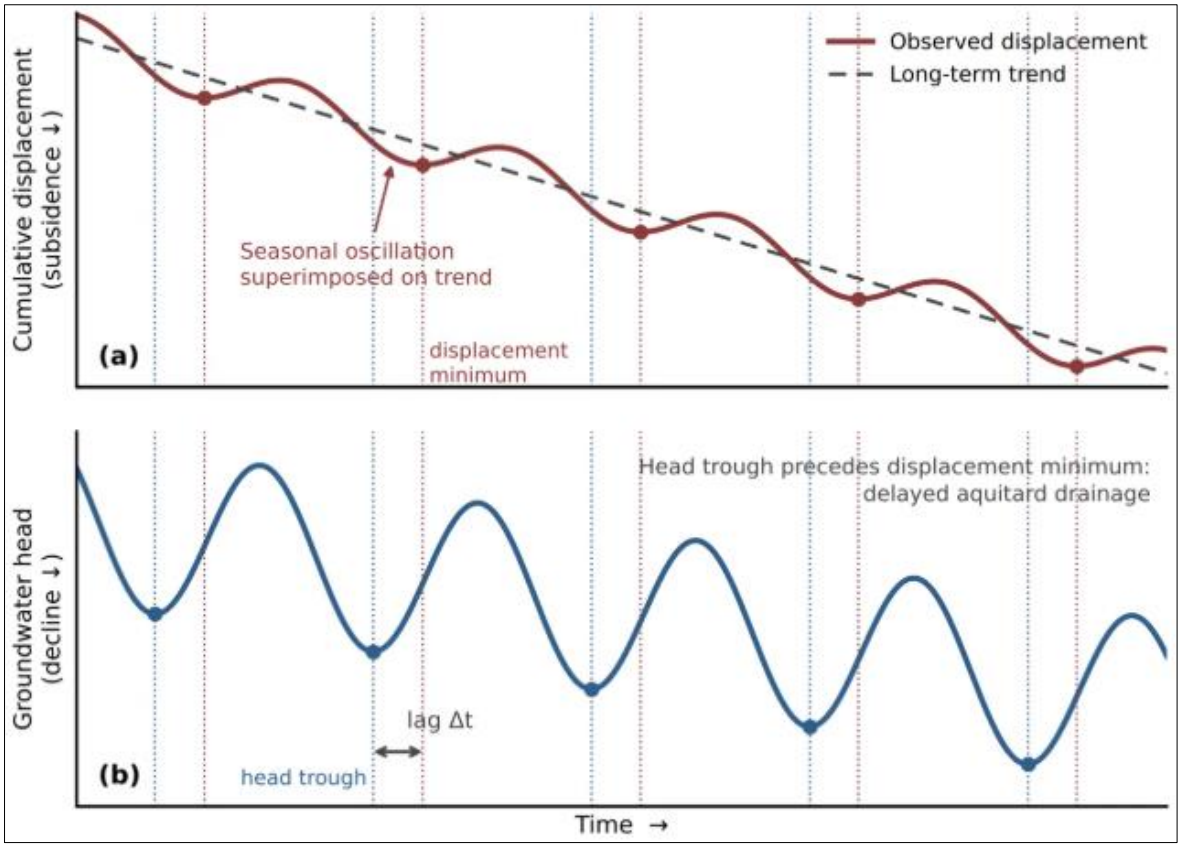

Fig 3: Conceptual time series of seasonal and long-term subsidence. A curve with a downward trend and superimposed seasonal oscillation. A second panel below shows the groundwater head hydrograph, with troughs preceding the displacement minima by a short lag, illustrating delayed aquitard drainage.

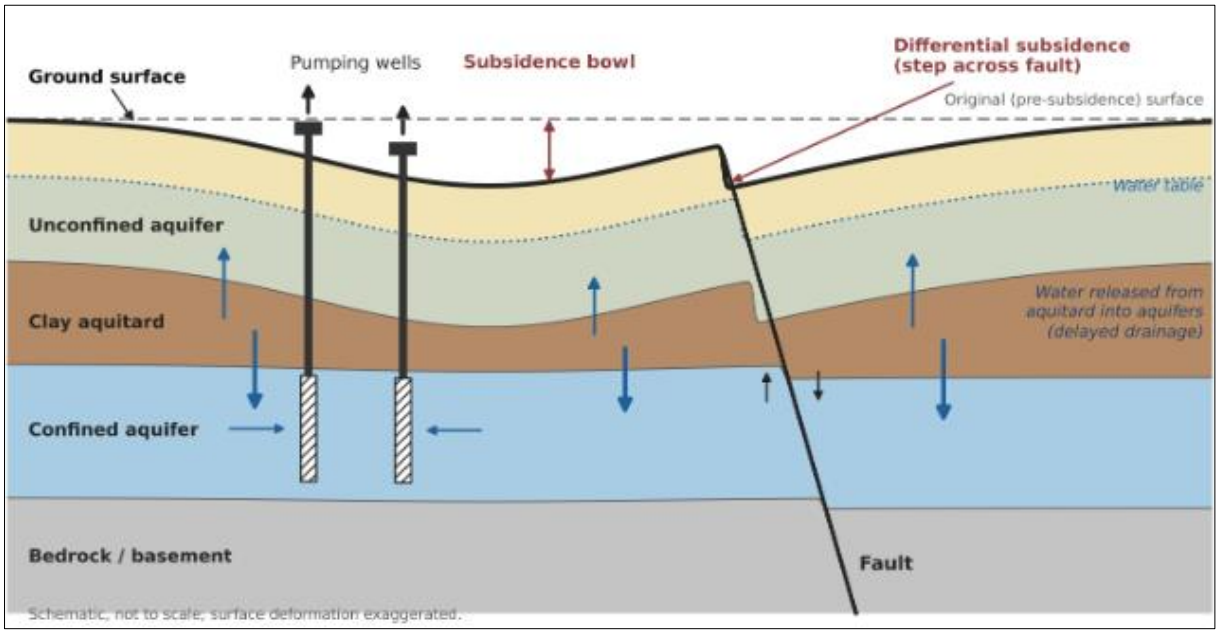

Fig 4: Cross-section of a subsiding aquifer system. A vertical profile showing the ground surface, an upper unconfined aquifer, a clay aquitard, a confined aquifer with pumping wells, and a fault. The surface profile above is drawn as a bowl with a sharp step across the fault, to illustrate differential subsidence. Arrows mark the direction of water flow from aquitard to aquifer.

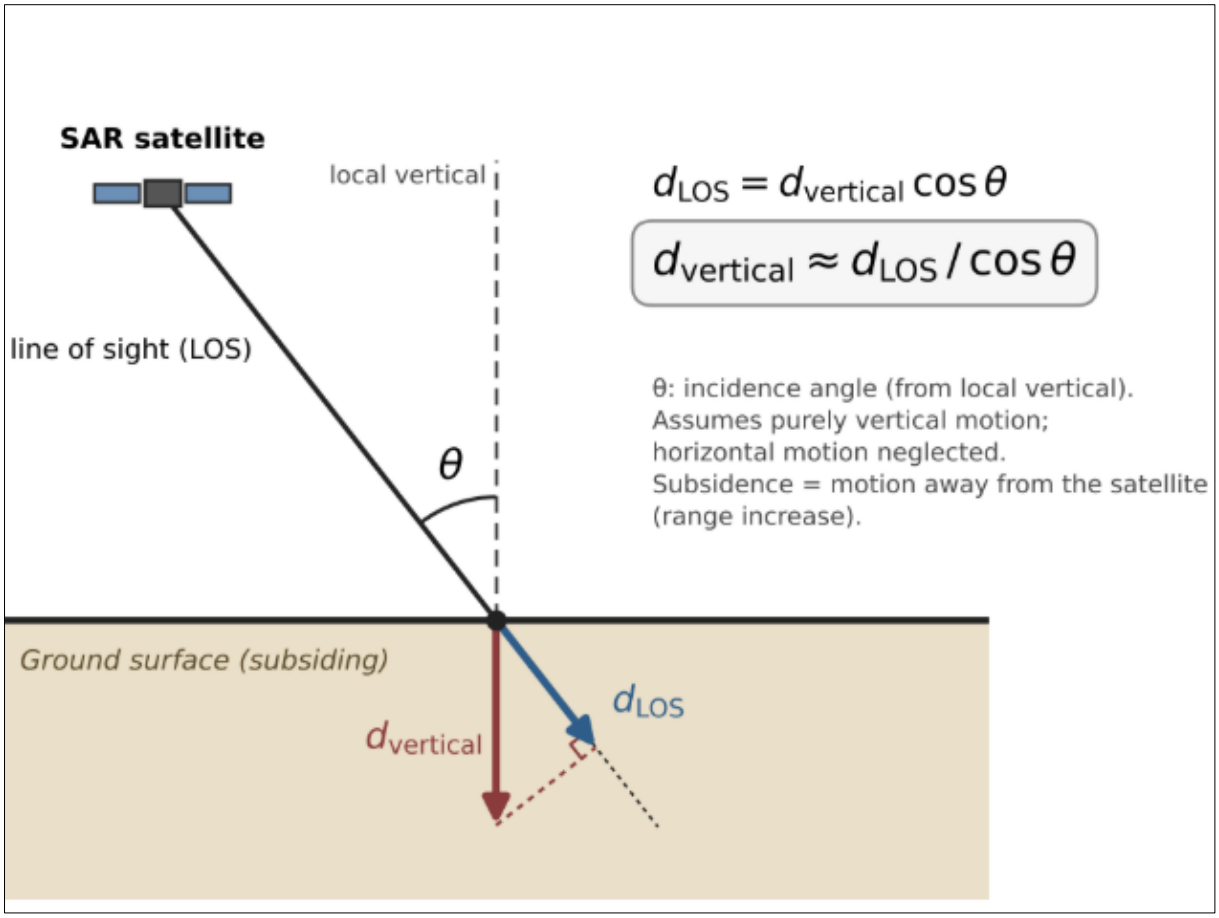

Fig 5: Radar geometry and line-of-sight projection. A satellite viewing the ground at incidence angle θ, with the vertical displacement vector and its LOS projection drawn on the surface. The relation d_vertical ≈ d_LOS / cos θ is printed alongside.

Conclusions

InSAR has changed how land subsidence from groundwater extraction is observed. It provides dense, repeatable, and increasingly free measurements that no ground network could match. Its greatest value emerges when displacement is interpreted through the physics of effective stress: the relationship between compaction and head decline separates elastic from inelastic behavior, reveals structural controls, and supports estimates of storage properties. The case studies reviewed here show that

deformation is strongest where heavy pumping meets thick compressible sediments, and that regulation can slow, but not reverse, the damage already done.

Reliable assessments need three things: rigorous error control, independent validation, and integration with hydrogeological data. When these are present, InSAR supports defensible hazard maps and head-based management thresholds. Future work should focus on combining multi-sensor and multi-geometry data, on longer-wavelength missions for farmland, and on coupling deformation observations with numerical groundwater models, so that subsidence can be forecast and not only mapped.

References

1. Amelung F, Galloway DL, Bell JW, Zebker HA, Laczniak RJ. Sensing the ups and downs of Las Vegas: InSAR reveals structural control of land subsidence and aquifer-system deformation. Geology. 1999;27(6):483-6.
2. Bell JW, Amelung F, Ferretti A, Bianchi M, Novali F. Permanent scatterer InSAR reveals seasonal and long-term aquifer-system response to groundwater pumping and artificial recharge. Water Resour Res. 2008;44:W02407.
3. Berardino P, Fornaro G, Lanari R, Sansosti E. A new algorithm for surface deformation monitoring based on small baseline differential SAR interferograms. IEEE Trans Geosci Remote Sens. 2002;40(11):2375-83.
4. Bürgmann R, Rosen PA, Fielding EJ. Synthetic aperture radar interferometry to measure Earth's surface topography and its deformation. Annu Rev Earth Planet Sci. 2000;28:169-209.
5. Chaussard E, Amelung F, Abidin H, Hong SH. Sinking cities in Indonesia: ALOS PALSAR detects rapid subsidence due to groundwater and gas extraction. Remote Sens Environ. 2013;128:150-61.
6. Chaussard E, Wdowinski S, Cabral-Cano E, Amelung F. Land subsidence in central Mexico detected by ALOS InSAR time-series. Remote Sens Environ. 2014;140:94-106.
7. Chen CW, Zebker HA. Two-dimensional phase unwrapping with use of statistical models for cost functions in nonlinear optimization. J Opt Soc Am A Opt Image Sci Vis. 2001;18(2):338-51.
8. Ferretti A, Prati C, Rocca F. Permanent scatterers in SAR interferometry. IEEE Trans Geosci Remote Sens. 2001;39(1):8-20.
9. Galloway DL, Hoffmann J. The application of satellite differential SAR interferometry-derived ground displacements in hydrogeology. Hydrogeol J. 2007;15(1):133-54.
10. Galloway DL, Jones DR, Ingebritsen SE. Land subsidence in the United States. Reston (VA): U.S. Geological Survey; 1999. Circular 1182.
11. Goldstein RM, Werner CL. Radar interferogram filtering for geophysical applications. Geophys Res Lett. 1998;25(21):4035-8.
12. Herrera-García G, Ezquerro P, Tomás R, Béjar-Pizarro M, López-Vinielles J, Rossi M, *et al*. Mapping the global threat of land subsidence. Science. 2021;371(6524):34-6.
13. Hoffmann J, Zebker HA, Galloway DL, Amelung F. Seasonal subsidence and rebound in Las Vegas Valley, Nevada, observed by synthetic aperture radar interferometry. Water Resour Res. 2001;37(6):1551-66.
14. Hooper A. A multi-temporal InSAR method incorporating both persistent scatterer and small baseline approaches. Geophys Res Lett. 2008;35:L16302.
15. Hooper A, Zebker H, Segall P, Kampes B. A new method for measuring deformation on volcanoes and other natural terrains using InSAR persistent scatterers. Geophys Res Lett. 2004;31:L23611.
16. Massonnet D, Feigl KL. Radar interferometry and its application to changes in the Earth's surface. Rev Geophys. 1998;36(4):441-500.
17. Motagh M, Walter TR, Sharifi MA, Fielding E, Schenk A, Anderssohn J, *et al*. Land subsidence in Iran caused by widespread water reservoir overexploitation. Geophys Res Lett. 2008;35:L16403.
18. Phien-wej N, Giao PH, Nutalaya P. Land subsidence in Bangkok, Thailand. Eng Geol. 2006;82(4):187-201.
19. Poland JF, editor. Guidebook to studies of land subsidence due to ground-water withdrawal. Paris: UNESCO; 1984.
20. Rodell M, Velicogna I, Famiglietti JS. Satellite-based estimates of groundwater depletion in India. Nature. 2009;460:999-1002.
21. Shirzaei M, Freymueller J, Törnqvist TE, Galloway DL, Dura T, Minderhoud PSJ. Measuring, modelling and projecting coastal land subsidence. Nat Rev Earth Environ. 2021;2:40-58.
22. Terzaghi K. Erdbaumechanik auf bodenphysikalischer Grundlage. Leipzig: Franz Deuticke; 1925.
23. Torres R, Snoeij P, Geudtner D, Bibby D, Davidson M, Attema E, *et al*. GMES Sentinel-1 mission. Remote Sens Environ. 2012;120:9-24.
24. Wada Y, van Beek LPH, van Kempen CM, Reckman JWTM, Vasak S, Bierkens MFP. Global depletion of groundwater resources. Geophys Res Lett. 2010;37:L20402.
25. Zebker HA, Villasenor J. Decorrelation in interferometric radar echoes. IEEE Trans Geosci Remote Sens. 1992;30(5):950-9.
26. Zhu L, Gong H, Li X, Wang R, Chen B, Dai Z, *et al*. Land subsidence due to groundwater withdrawal in the northern Beijing plain, China. Eng Geol. 2015;193:243-55